Metabolism is the major driver of hydrogen isotope fractionation recorded in tree-ring glucose of *Pinus nigra*

Thomas Wieloch[a,*], Michael Grabner[b], Angela Augusti[c], Henrik Serk[a], Ina Ehlers[a], Jun Yu[d], Jürgen Schleucher[a]

[a] Department of Medical Biochemistry and Biophysics, Umeå University, 901 87 Umeå, Sweden

[b] Institute of Wood Technology and Renewable Materials, University of Natural Resources and Life Sciences Vienna, 3430 Tulln an der Donau, Austria.

[c] Research Institute on Terrestrial Ecosystems, National Research Council, 05010 Porano (TR), Italy.

[d] Department of Mathematics and Mathematical Statistics, Umeå University, 901 87 Umeå, Sweden

* To whom correspondence may be addressed (thomas.wieloch@umu.se, +46706460369)

Main body of the text: 6333 words

Summary: 147 words

Introduction: 856 words

Materials and Methods: 561 words

Results: 2957 words

Discussion: 1959 words

4 Figures (all colour), 3 Tables (Table 1 and 2 in colour), Supporting information (SI 1 to 8)

Author	Email address	ORCID
Thomas Wieloch	thomas.wieloch@umu.se	0000-0001-9162-2291
Michael Grabner	michael.grabner@boku.ac.at	0000-0002-5220-721X
Angela Augusti	angela.augusti@cnr.it	0000-0002-9591-693X
Henrik Serk	henrik.serk@umu.se	0000-0003-4803-3664
Ina Ehlers	ina.ehlers@gmail.com	
Jun Yu	jun.yu@umu.se	0000-0001-5673-620X
Jürgen Schleucher	jurgen.schleucher@umu.se	

Summary

- Stable isotope abundances convey valuable information about plant physiological processes and underlying environmental controls. Central gaps in our mechanistic understanding of hydrogen isotope abundances impede their widespread application within the plant and Earth sciences.

- To close these gaps, we analysed intramolecular deuterium abundances in glucose of *Pinus nigra* extracted from an annually resolved tree-ring series (1961 to 1995).

- We found fractionation signals at glucose H^1 and H^2 introduced by closely related metabolic processes. These signals (and thus metabolism) respond to drought and atmospheric CO_2 concentration beyond a response change point. They explain ≈60% of the whole-molecule deuterium variability. Altered metabolism is associated with below-average yet not exceptionally low growth.

- We propose the signals are introduced at the leaf-level by changes in sucrose-to-starch carbon partitioning and anaplerotic carbon flux into the Calvin-Benson cycle. In conclusion, metabolism can be the main driver of hydrogen isotope variation in plant glucose.

Keywords: anaplerotic flux; Calvin-Benson cycle; change point; glucose-6-phosphate shunt; hydrogen stable isotopes; intramolecular isotope analysis; oxidative pentose phosphate pathway; sucrose-to-starch carbon partitioning

Introduction

Stable isotope measurements of the most abundant chemical elements in plants (H, C, and O) convey valuable information about plant physiological and environmental processes. Plant archives, such as tree rings, preserve this information over millennia enabling elucidation of physiological and environmental dynamics that occur beyond the short timeframes covered by manipulation or monitoring experiments (Peñuelas *et al.*, 2011; Loader *et al.*, 2011; Saurer *et al.*, 2014; Frank *et al.*, 2015; Köhler *et al.*, 2016).

Among all stable isotopes, the hydrogen isotopes protium (^{1}H) and deuterium (^{2}H, or D) exhibit the largest relative mass difference. As a result, hydrogen isotope effects are normally considerably larger than isotope effects of other elements (Melander & Saunders, 1980). Thus, from the physics point of view, hydrogen isotope compositions of plant compounds (commonly expressed in terms of δD) have a remarkable potential to further our knowledge about plant physiological and environmental processes. However, current plant δD models fail to predict the entire body of available empirical data (Waterhouse *et al.*, 2002). Therefore, hydrogen isotopes, in contrast to carbon and oxygen isotopes, have not yet evolved into standard tools within the plant and Earth sciences.

Current δD models of plant organic matter exhibit three main components: (i) the δD composition of plant water sources, (ii) leaf water D enrichment, and (iii) metabolic fractionations. (i) Plants take up soil water through roots. In most plants, this uptake and water transport through the xylem into leaves occurs without detectable δD shifts (Cernusak *et al.*, 2016). In addition, leaf water exchanges with atmospheric water vapour through stomata. Thus, leaf water inherits the δD compositions of both soil water and atmospheric water vapour (Cernusak *et al.*, 2016). (ii) Stomatal evaporation causes D enrichments in leaf water. Adaptations of the Craig-Gordon model describe this process at the site of evaporation (Craig & Gordon, 1965; Flanagan *et al.*, 1991; Farquhar *et al.*, 2007). In a comprehensive series of gas exchange experiments over a range of isotopic and humidity conditions far exceeding natural conditions, Roden and Ehleringer (1999a) confirmed the robustness of a model that approximates leaf water D enrichment (Flanagan *et al.*, 1991). Similarly, on an extensive δD dataset of leaf waters from very dry to very wet field sites, Kahmen *et al.* (2013) confirmed the robustness of the precise δD enrichment model (Farquhar *et al.*, 2007). Reanalysing this latter dataset, Cernusak *et al.* (2016) reported a goodness of fit of R^2=0.92 (n=332) between modelled and measured δD data. These successful tests for robustness of leaf water δD models strongly

suggest that inconsistencies between modelled and measured δD values of plant organic matter as reported by Waterhouse *et al.* (2002) derive from processes that occur downstream of leaf water D enrichment, i.e., from fractionating metabolic processes. (iii) To predict δD values of tree-ring cellulose, Roden *et al.* (2000) expanded a leaf water δD model (Flanagan *et al.*, 1991) by a term accounting for δD changes due to the partial reincorporation of hydrogen from xylem water during cellulose biosynthesis (=heterotrophic hydrogen exchange). Furthermore, Roden *et al.* (2000) added two constants accounting for D fractionations by unspecified autotrophic and heterotrophic metabolic processes. Roden and Ehleringer (1999b, 2000) confirmed the robustness of their model for greenhouse- and field-grown riparian trees with good access to water. A robustness test by Waterhouse *et al.* (2002) on tree rings of *Quercus robur* from a dry site failed. These latter authors suggested that modelling metabolic fractionations as constants may be inadequate.

All hydrogen positions of leaf-level metabolites inherit D fractionation signals present in leaf water, the hydrogen source of metabolism. By contrast, metabolic reactions cause D fractionations at specific–intramolecular–hydrogen positions that are directly or indirectly involved in the reaction mechanism (Schmidt *et al.*, 2015). Such fractionations are known to result in pronounced δD differences among hydrogen positions within a metabolite (Martin *et al.*, 1986; Schleucher, 1998; Schmidt *et al.*, 2003). In addition, it is now known that metabolic δD variability can occur at a given intramolecular hydrogen position (Schleucher, 1998). Specifically, δD changes at H^6 of plant leaf glucose were shown to reflect changes of the photorespiration-to-photosynthesis ratio (Schleucher, 1998; Ehlers *et al.*, 2015). Moreover, growing six C_3 species at ambient CO_2 concentrations of 280 and 150 ppm, Cormier *et al.* (2018) reported whole-molecule δD differences of ≈20‰ (on average) in leaf α-cellulose caused by so far unknown fractionating metabolic processes. This shows that the predictive abilities of plant δD models will improve by accounting for variability in metabolic fractionations. To this end however, underlying mechanisms need to be elucidated.

Since deuterium fractionations by metabolic processes occur at specific hydrogen positions within molecules, conventional whole-molecule isotope data have a limited interpretability. For instance, not knowing the intramolecular location of metabolic fractionation impedes attempts to elucidate its enzymatic origin. In addition, if located at a single hydrogen position, a ≈20‰ whole-molecule effect as reported by Cormier *et al.* (2018) scales up to ≈140‰ because glucose monomers of α-cellulose have seven H-C positions (Fig. 1). For a better understanding of

metabolic fractionations and underlying processes in highly relevant systems (plant archives), we here analysed intramolecular D abundances in tree-ring glucose of the gymnosperm *Pinus nigra*.

Material and Methods

Site and samples

The sampling site and samples were described previously (SI 1) (Leal *et al.*, 2008; Wieloch *et al.*, 2018).

Intramolecular deuterium measurements

Intramolecular D abundances were measured following a published protocol (Betson *et al.*, 2006). Quantitative D NMR spectra were recorded using an AVANCE III 850 with a cryogenic probe optimised for D detection and ^{19}F lock (Bruker BioSpin GmbH, Rheinstetten, Germany). Relative intramolecular D abundances were determined by signal deconvolution using Lorentzian line shape fits in TopSpin 4 (Bruker BioSpin GmbH, Rheinstetten, Germany). 3,6-anhydro-1,2-*O*-isopropylidene-α-D-glucofuranose has six methyl-group hydrogens which were introduced during derivatisation and derive from a common batch of acetone. We used their average D abundance as reference to compare glucose D abundances of tree-ring samples from different years. Thus, we expressed tree-ring data as $\delta D_i=(D_i/(\Sigma D_{ME}/6)-1)*10^3$ with D_i and D_{ME} denoting relative D abundances at glucose H-C positions (Fig. 1) and the methyl-group hydrogens, respectively. Note that *i* corresponds to the H-C designation of glucose, not its derivative used for NMR measurements.

Metabolic fractionation at glucose H^1 and H^2, ε_{met}

We estimated metabolic fractionation at glucose H^1 and H^2 combinedly as $\varepsilon_{met}=(1/2\Sigma(D_1, D_2)/1/5\Sigma(D_3, D_4, D_5, D_{6S}, D_{6R})-1)*10^3$. This procedure maximises metabolic fractionation signals located at H^1 and H^2 and minimises signals of fractionating processes that affect all H-C positions equally, such as leaf water D enrichment, or similarly, such as the soil water D abundance.

Environmental data

Monthly resolved data of precipitation, air temperature, sunshine duration, global radiation, and relative humidity were measured at the climate station Hohe Warte (WMO ID: 1103500). Air vapour pressure deficits were calculated according to standard procedures. We used monthly

resolved datasets of the self-calibrating Palmer drought severity index and the standardised precipitation-evapotranspiration index for 48.25N, 16.25E (Wells *et al.*, 2004; Vicente-Serrano *et al.*, 2010). Annual atmospheric CO_2 concentrations were measured at the Mauna Loa observatory, Hawaii by Pieter Tans (NOAA/ESRL, USA) and Ralph Keeling (Scripps Institution of Oceanography, USA). Both the selected grid point and climate station are no more than a horizontal distance of 15 km from the sampling site with a negligible vertical offset. CO_2 is well mixed in the atmosphere. Thus, all data should represent the site conditions well.

Variance contribution of δD_i to δD_g

We calculated the variance contribution of each δD_i to δD_g as follows (Fig. 2d). With $\delta D_g = 1/7 \Sigma \delta D_i$, the variance of δD_g equals the covariance average between δD_i and δD_g as $Var(\delta D_g) = 1/7 \Sigma Cov(\delta D_i, \delta D_g)$. Thus, percent variability contributions of δD_i to δD_g are given as $VC_i = 1/7 Cov(\delta D_i, \delta D_g)/Var(\delta D_g)*100$. For this calculation we only used years without any missing data (n=8*25, see outlier treatment above).

Statistical analyses

Hierarchical cluster analysis was performed using the R function hclust() of the STATS package on z-scores of δD_i using Euclidean distances and Ward's fusion criterion for cluster formation (n=7*31). Mood's median tests were performed using the R function median_test() of the COIN package. Batch change point analysis based on the non-parametric Mann-Whitney-Wilcoxon test was performed using the R function detectChangePointBatch() of the CPM package (Ross, 2015). Multiple linear regression modelling was performed using the R function lm() of the STATS package. Change point regression modelling (step type) was performed using the R function chngptm() of the CHNGPT package (Fong *et al.*, 2017). Statistical significances of the change point and the change point model were calculated using the R functions chngpt.test() of the CHNGPT package and lrtest() of the LMTEST package, respectively.

Results

Data and site description

To better understand metabolic fractionations, we measured intramolecular D abundances at all seven H-C positions of glucose extracted across an annually resolved *Pinus nigra* tree-ring series (Fig. 1). Our timeseries covers the period 1961 to 1995 but lacks data for 1977, 1978, 1981 and 1982. Hence, the raw dataset consists of seven intramolecular δD_i timeseries each

comprising 31 observations (n=7*31=217). In addition, we derived the molecular average timeseries, δD_g (n=31). Samples were taken at a site in the Vienna basin (Austria) with very dry and shallow soil, an open canopy, and apparently low competition among trees (Strumia *et al.*, 1997; Wimmer *et al.*, 2000; Leal *et al.*, 2007, 2008; Wieloch *et al.*, 2018). Sampling targeted dominant trees with drought habitus.

In preparation of our data analysis, we performed an outlier analysis. Outliers can potentially impair statistical analyses because they may reflect either experimental errors or extreme states of the system. Since we were interested in the normal functioning of plant metabolism and metabolic fractionation, we removed outliers to ensure robust results. We identified outliers in δD_i timeseries as values that were 1.5 times the interquartile range below the first or above the third quartile. We removed one data point each from δD_4 and δD_5 (n=30), three data points from δD_{6R} (n=28) and five data points from δD_{6S} (n=26) resulting in six missing data points in δD_g (n=25). Average standard errors of δD_i and δD_g measurements are 5.4‰ and 3.4‰, respectively.

δD_1 and δD_2 reflect highly variable and closely related metabolic processes

Intramolecular D abundances of *Pinus nigra* tree-ring glucose differ among H-C positions (Figs. 1, 2b, and S2b). Medial intramolecular differences exceed 225‰ (δD_1 vs. δD_{6S}) and differences of similar magnitude have been reported previously (Schleucher, 1998; Schleucher *et al.*, 1999; Augusti *et al.*, 2006, 2008; Betson *et al.*, 2006; Ehlers *et al.*, 2015). This shows that metabolic fractionations, being position-specific, have strong effects. Interestingly, in some years, intramolecular δD differences approach 450‰ (Fig. S2b). Thus, metabolic fractionations are highly variable on the interannual scale.

Hierarchical cluster analysis (HCA) groups timeseries according to co-variability. Timeseries carrying common signals, i.e., information about a common process or strongly related processes, form clusters. Performing HCA on our δD_i dataset, we found a strong separation between a cluster comprising δD_1 and δD_2 and a cluster comprising δD_3 to δD_{6R} (Fig. 2a). In addition, we found separations within the δD_3 to δD_{6R} cluster, with δD_4 showing the highest degree of independency. Thus, δD_i timeseries carry information about several ecophysiological processes.

While δD_3 to δD_{6R} exhibit similar degrees of variability (Fig. 1; *SD*=±10.5‰ to ±16.8‰, range=42‰ to 63‰, *n*=26 to 31), δD_2 varies considerably (*SD*=±91.8‰, *range*=300‰, *n*=31) and δD_1 is also relatively variable (*SD*=±28.4‰, *range*=99‰, *n*=31). Increased D variability at two out of seven H-C positions suggests that metabolic fractionations occur at these positions, H^1, and H^2.

To further investigate this, we performed HCA on annual δD_i patterns and found two groups (SI 2). Figure 2b shows the arithmetic average patterns of both groups. While δD_3 to δD_{6R} values remain comparably constant under all conditions experienced by the trees, δD_1 and δD_2 separate annual δD_i patterns into a low-value group (black, *n*=22) and a high-value group (green, *n*=9). According to one-tailed Student's t-tests, δD_1 and δD_2 increases are statistically significant (δD_1: 54‰ on average, $p<10^{-9}$; δD_2: 186‰ on average, $p<10^{-4}$). According to one-tailed Mood's median tests, median increases are statistically significantly as well ($p<.001$). Since differences in δD_i patterns reflect differences in metabolism, this finding confirms that glucose H^1 and H^2 carry metabolic fractionation signals. Underlying metabolic processes are closely related (Fig. 2a).

Since the high-value group exhibits more pronounced intramolecular δD_i patterns than the low-value group (Figs. 2b, and S2b), metabolic shifts are probably associated with high δD_1 and δD_2 values. To further investigate this, we performed major axis regression analysis on low and high δD_1 and δD_2 values (Fig. 2c, black and green circles, respectively). Compared to ordinary least squares regression analysis, major axis regression analysis yields truer parameter estimates when x-variable data contain significant relative errors as is the case here for low-value data. For low values, we found a slope of ≈0.81 with a 95% confidence interval of ≈0.60 to ≈1.07 (*n*=22), i.e., δD_1 and δD_2 increase at a ≈1:1 ratio. For high values, we found a slope of ≈0.16 with a 95% confidence interval of ≈0.07 to ≈0.25 (*n*=9), i.e., δD_1 and δD_2 increase at a ≈1:6 ratio. Non-metabolic fractionation processes have equal effects on all δD_i and can be expected to yield slopes=1. Thus, while δD_1 and δD_2 variability in the low-value range is consistent with non-metabolic fractionation processes, high values reflect additional effects by metabolic fractionation processes.

Metabolism changes in response to dry conditions after a change point is crossed

In general, the fractionating metabolic processes may be under developmental control. However, formation of tree rings analysed here occurred when the trees had reached a stable

canopy position. On average, tree-ring width measurements of the samples reach back to 1865 (*range*: 1840 to 1918) and δD_i timeseries start at 1961. Thus, the fractionating metabolic processes can be expected to be controlled by environmental parameters. In the following, these are elucidated in six steps which motivate two integrated isotope-environment models presented subsequently.

Step 1. Increases of metabolic fractionations at glucose H^1 and H^2 are temporally confined to the second part of the study period (Fig. 2c, 1983 to 1993). This may indicate the presence of a response change point. To test this, we estimated the average metabolic fractionation at glucose H^1 and H^2, ε_{met}, (see 'Material and Methods') and performed a batch change point analysis based on the non-parametric Mann-Whitney-Wilcoxon test (Ross, 2015). We found a change point at 1980 (p<.001, n=31) showing that the observed frequency distribution of ε_{met} (Fig. S3a) does not align with the properties of a single theoretical probability distribution. That is, ε_{met} data of 1961 to 1980 and 1983 to 1995 follow different probability distributions (1981 and 1982 are missing). Thus, the ε_{met} timeseries exhibits a change point beyond which the fractionating metabolic processes are activated or upregulated.

Step 2. Upregulation of the fractionating metabolic processes occurs beyond a change point. Below the change point, environmental variability exerts no control (Fig. 2c, 1:1 ratio). To investigate when the change point is crossed, we correlated ε_{met} with different climate parameters: air vapour pressure deficit, *VPD*; precipitation, *PRE*; the self-calibrating Palmer drought severity index, *PDSI* (Wells *et al.*, 2004); air temperature, *TMP*; sunshine duration, *SD*; global radiation, *RAD*; atmospheric CO_2 concentrations, C_a; and the standardised precipitation-evapotranspiration index, *SPEI* (Vicente-Serrano *et al.*, 2010). Since ε_{met} does not follow a normal distribution (Fig. S3a), we calculated Spearman's rank correlation coefficient, ρ. Our analysis included four time periods: January to December, year; March to May, spring; March to November, growing season (Wieloch *et al.*, 2018); and June to July, summer. For most periods, we found significant positive correlations of ε_{met} with *VPD* and significant negative correlations with *PDSI* and *SPEI* (Table 1). High *VPD*, low *PDSI*, and low *SPEI* correspond to dry conditions. Thus, the results indicate that upregulation of the fractionating metabolic processes (high ε_{met}) occurs in response to dry conditions. This response is consistent with the reported positive offsets between measured tree-ring δD data of *Quercus robur* from a dry site and model predictions that assume 43% heterotrophic hydrogen exchange (Waterhouse *et al.*, 2002) as reported for the same genus (Augusti *et al.*, 2006).

Step 3. SPEI can be calculated for different timescales reflecting different drought types (Vicente-Serrano *et al.*, 2010). While short timescales chiefly reflect variability in soil moisture, long timescales reflect variability in groundwater storage (Vicente-Serrano *et al.*, 2010). To investigate effects of different drought types on the fractionating metabolic processes, we correlated ε_{met} with *SPEI* calculated for timescales of 1, 3, 4, 6, 8, 12, 16, 24, 36, and 48 months. We found increasing correlation coefficients from short to long timescales indicating that long-term drought reflecting depleted groundwater storage promoted upregulations of the fractionating metabolic processes (Table 1). Long-term drought events have a low temporal frequency (Vicente-Serrano *et al.*, 2010). This may explain why upregulations of the fractionating metabolic processes occurs not scattered over the entire study period but over consecutive years during the second half of the study period (Fig. 2c).

Step 4. In addition to correlations indicative of drought control, we found a significant positive correlation between ε_{met} and C_a (Table 1) which, most likely, constitutes a pseudocorrelation resulting from intercorrelation between C_a and long-term drought (Pearson correlation between C_a and the growing season 48-months *SPEI*: r=-0.83, $p<10^{-7}$, n=31). For the year and spring, we found significant positive correlations between ε_{met} and *TMP* (Table 1). Thus, air temperature may contribute to upregulations of the fractionating metabolic processes. Alternatively, the *TMP* correlation may be explained by intercorrelation with drought parameters. Furthermore, we considered pathogens as cause for upregulations of the fractionating metabolic processes. The Research Centre for Forests (Vienna, Austria) closely monitors and reports on pathogen status. To our knowledge, there are no reports of major damage by pathogens for the studied *Pinus nigra* stand during the 1980's and early 1990's. Thus, significant effects of pathogens on upregulations of the fractionating metabolic processes are unlikely. Similarly, effects by forest management interventions are unlikely since the stand is not used economically (Leal *et al.*, 2008). Effects by air pollutants could not be assessed due to limited data availability.

Step 5. Analysing expressions of *SPEI* values enables assessments of drought severity as ≥-0.49, non-drought; -0.5 to -0.99, mild drought; -1 to -1.49, moderate drought; -1.5 to -1.99, severe drought; and <-2, extreme drought (McKee *et al.*, 1993; Paulo *et al.*, 2012). To assess the magnitude of the drought shift indicated by correlation, we plotted the growing-season 48-months *SPEI* as function of time (Fig. 3a). Trendline analysis shows a significant increase in

drought severity with a long-term shift from "non-drought" from 1961 to 1978, to "mild drought" from 1979 to 1988, to "moderate drought" from 1989 to 1995 (R^2=0.69, $p<10^{-9}$, n=35). Thus, upregulations of the fractionating metabolic processes in between 1983 and 1993 occurred when the study region experienced mild to moderate drought. Note that actual conditions at the site may have deviated from regional conditions plotted in figure 3a.

Step 6. Figure 3a indicates that during the growing seasons of 1994 and 1995 groundwater storage was exceptionally low. However, this did not result in significant upregulations of the fractionating metabolic processes (Fig. 2c). Therefore, we hypothesise that the long-term depletion of the groundwater storage below a critical level is merely setting the stage for upregulation and that secondary climate factors exert control on shorter timescales. To investigate this, we repeated the ε_{met}-climate-correlation analysis with data of the second half of the study period, 1983 to 1995. We justify this data selection as follows. In 1983, upregulation of the fractionating metabolic processes occurred for the first time (Fig. 2c). From 1983 to 1995, long-term groundwater storage kept decreasing (Fig. 3a, dotted black line). Thus, it can be expected that site conditions during this period were generally favourable for upregulation. Before 1983, groundwater storage was higher and may thus have rendered the upregulation impossible (Fig. 3a). In this scenario, control by secondary climate factors would have been impossible and considering their variability would impair correlation results. Since the selected subset of ε_{met} (1983 to 1995) follows a normal distribution (Fig. S3b), we calculated Pearson correlation coefficients, r. We found significant negative correlations between ε_{met} and *PRE* (Table 2). Under generally dry conditions, low precipitation can be expected to result in low soil moisture. Thus, the results indicate that upregulations of the fractionating metabolic processes (high ε_{met}) occurred in response to short-term depletions in soil moisture when groundwater storage was below the critical level. In this respect, it is noteworthy that *Pinus nigra* reportedly has a well-developed lateral root system in upper soil layers to access soil water but can additionally tap into deep water sources if available (Stokes *et al.*, 2002; Peñuelas & Filella, 2003). Furthermore, we found a significant negative correlation between ε_{met} and annual C_a (Table 2). This correlation is not explained by intercorrelation between C_a and long-term drought (Pearson correlation between C_a and the growing season 48-months *SPEI*: r=-0.39, p>.1, n=13). Thus, the result indicates that high atmospheric CO_2 concentrations counteracted upregulations of the fractionating metabolic processes (high ε_{met}) when groundwater storage was below the critical level.

Model 1. To further corroborate the existence of a response change point (step 1), and the requirement of a depletion in groundwater storage (steps 2, and 3) for the manifestation of effects by secondary climate factors (step 6) we modelled two ε_{met} groups as functions of *PRE* and C_a as $\varepsilon_{met}=\alpha_1+\alpha_2 PRE+\alpha_3 C_a$. While the first group includes data of 1961 to 1982 corresponding to high groundwater storage, the second group includes data of 1983 to 1995 corresponding to low groundwater storage (Fig. 3a). For the latter group, we found adequate linear models including, as explanatory variables, spring *PRE* and annual C_a (R^2=0.74, p<.01, n=13), and summer *PRE* and annual C_a (R^2=0.78, p<.001, n=13). The most adequate model we found includes summed spring and summer *PRE* and annual C_a (R^2=0.87, $p<10^{-4}$, n=13, α_1=1801.97, α_2=-0.566, α_3=4.1851; see Figs. S4a, and b for bivariate relationships of ε_{met} with *PRE* and C_a, respectively). Both *PRE* and C_a contributed significantly to all models (p<.05). For ε_{met} data of the first group, 1961 to 1982, the most adequate model has no explanatory power (p>.1, n=18). Modelling ε_{met} by the most adequate model works well for the second group, 1983 to 1995, yet produces large offsets between all measured and modelled values of the first group (Fig. 3b). This corroborates that (i) a response change point exists, and (ii) the manifestation of effects by secondary climate factors requires a depletion in groundwater storage. Furthermore, it should be noted that the most adequate model accounts well for low ε_{met} values in 1994 and 1995 (Fig. 3b). During these years, groundwater storage was exceptionally low, yet *PRE* and C_a were high (Figs. 3a, S4a, and S4b). Thus, depleted groundwater storage alone does not necessarily lead to an upregulation of the fractionating metabolic processes. High precipitation during spring and summer as well as high atmospheric CO_2 concentrations exert counteracting effects.

Model 2. Above, we present evidence for several properties of ε_{met} of *Pinus nigra* tree-ring glucose. To test these properties in an integrated way and to estimate the change point value, we fitted a change point model to the entire dataset (Fong *et al.*, 2017). It takes the form $\varepsilon_{met}=\beta_1+\beta_2 z_1+\beta_3 z_2+\beta_4 I(x>e)+\beta_5 z_1 I(x>e)+\beta_6 z_2 I(x>e)$ where β_1 to β_6 are model coefficients, z_1 is March to June precipitation, z_2 is annual atmospheric CO_2 concentration, x is the trend of the growing season 48-months *SPEI* used as change point variable (Fig. 3a, dotted black line), and e is the change point value. If x>e then I(x>e) equals 1, else I(x>e) equals 0. The fitted model explains 94% of the variability in ε_{met} and is highly significant ($p<10^{-15}$, n=31). All explanatory variables and the change point contribute significantly (Table 3). The estimated change point is at -0.7 ± 0.05SE corresponding to mild long-term drought ($p<10^{-15}$, Table 3, Fig. 3a). The presence/absence and directionality of modelled ε_{met} relationships with precipitation and

atmospheric CO_2 concentration agree with results given above (Tables 1-3). In contrast to the model without response change point (Fig. 3b), the change point model captures the variability of the entire ε_{met} dataset (Fig. 3c). Thus, this integrated change point model confirms the following findings. First, ε_{met} exhibits a response change point. Below this change point, ε_{met} is largely constant with values of ≈96‰. Above the change point, ε_{met} variability is high. Second, crossing the response change point requires a decrease in groundwater storage below a critical level. Third, March to July precipitation reflecting soil moisture and annual atmospheric CO_2 concentration govern ε_{met} variability on short timescales when groundwater storage is below the critical level.

Variability in δD_g is predominantly controlled by fractionating metabolic processes

Metabolic fractionations in δD_1 and δD_2 have a strong weight on whole-molecule D variability, δD_g. Variance partitioning shows that δD_1 and δD_2 together account for 71% of the variance in δD_g (Fig. 2d). By contrast, δD_3 to δD_{6R} each account for 5.8% on average. Assuming the variability in δD_3 to δD_{6R} reflects the combined influence of known fractionation processes affecting all δD_i, such as leaf water D enrichment, metabolic fractionations in δD_1 and δD_2 together account for 59.4% of the variance in δD_g (71%-2*5.8%). When years affected by metabolic fractionation are considered exclusively (green dots in Fig. 2c), metabolic fractionations in δD_1 and δD_2 together account for 74.2% of the variance in δD_g (SI 5). After excluding the period affected by metabolic fractionation from the analysis (1983 to 1995), all δD_i exhibit similar degrees of variance and contribute similarly to δD_g (SI 6) consistent with expectations related to known fractionation processes. Thus, in the present case, δD_g variability is predominantly controlled by fractionating metabolic processes unaccounted for in current models.

Altered metabolism is associated with below-average yet not exceptionally low growth

Metabolic changes as reflected by changes in metabolic fractionation may impact on growth. To test this, we investigated the relationship between ε_{met} and tree-ring width. We found that when the fractionating metabolic processes were upregulated, significantly more narrow tree rings were formed compared to when they were downregulated (Fig. 3d, one-tailed t-test: green vs. black circles, 0.75 vs. 0.99 mm, $p<.05$, $n=9$ and 22). Thus, altered metabolism is associated with below-average growth. However, equally narrow tree rings were formed in >50% of the years in which the fractionating metabolic processes were downregulated (Fig. 3d; tree-ring

widths <0.99 mm, n=12). Thus, upregulations of the fractionating metabolic processes are not associated with exceptional growth declines.

Discussion

The role of leaf intercellular CO_2 concentrations

Upregulations of the fractionating metabolic processes occur in response to drought, yet high atmospheric CO_2 concentrations exert counteracting effects (Tables 1-3, Figs. 3a-c). Isohydric plant species such as *Pinus nigra* respond to drought by closing their stomata (Sade *et al.*, 2012). This impedes CO_2 uptake and promotes low intercellular CO_2 concentrations, C_i. By contrast, increasing C_a promotes increasing C_i. Thus, upregulations of the fractionating metabolic processes may be mediated by low C_i. In principle, whole-molecule stable carbon isotope ratios of plant organic matter, $\delta^{13}C$, enable C_i estimations because ^{13}C fractionation during carbon uptake is related to C_i/C_a (Farquhar *et al.*, 1982; Evans *et al.*, 1986). However, processes that are independent of carbon uptake fractionation exert strong control over $\delta^{13}C$ values of the samples studied here (Wieloch *et al.*, 2018, 2021a,b). Therefore, we decided against using $\delta^{13}C$-derived C_i estimates to test this hypothesis.

ε_{met}: An isotope biomarker reports metabolic changes and drought

Here, we report an isotope biomarker (ε_{met}) reflecting changes in plant metabolism. The two-state property is this biomarker's unique feature enabling unambiguous identification of alternate metabolic states. By contrast, other biomarkers develop in a purely continuous manner with indistinct transitions between states hindering attempts to ascertain plant functioning. While the mechanisms behind other biomarkers in plant archives often remain elusive, ε_{met} can be linked to specific physiological processes (see below). Upon their elucidation, ε_{met} may help to find plants with the makeup to support crucial ecosystem services such as food and resource security.

In *Pinus nigra* studied here, atmospheric CO_2 concentrations and drought exert control over ε_{met} (Tables 1-3, Figs. 3a-c). Since past atmospheric CO_2 concentrations are known, ε_{met} of tree-ring glucose may become a powerful proxy of drought affecting plant metabolism. *Pinus nigra* can access water from upper soil layers as well as from deep water sources (Stokes *et al.*, 2002; Peñuelas & Filella, 2003). Accordingly, metabolic responses to short-term drought events require a groundwater depletion (Tables 1-3, Figs. 3a-c). Thus, ε_{met} of *Pinus nigra* reports long-term drought events. However, tree species differ in their capabilities to access groundwater

storages and hence in their susceptibility to different drought types. Thus, species with or without groundwater access may provide information about long and short-term drought events, respectively.

Stable isotope methodology

Independent D signals identified at the intramolecular level constitute independent channels of physiological and environmental information (Fig. 2a). For instance, positive correlations between leaf water D enrichment (affecting all glucose H-C positions equally) and drought are common (Cernusak *et al.*, 2016). Here, we report positive correlations between metabolic D enrichments at tree-ring glucose H^1 and H^2, ε_{met}, and drought (Tables 1-3, Figs. 3a-c). Thus, these processes have overlapping effects and signal deconvolution requires the intramolecular approach. Therefore, we recommend the use of intramolecular rather than whole-molecule D analysis. This may enable the deconvolution of information about source water D abundance, leaf water D enrichment, heterotrophic hydrogen exchange, the photorespiration-to-photosynthesis flux ratio, and metabolic processes introducing signals reported here. Additionally, intramolecular D analysis may yield deconvoluted information about environmental and developmental controls of these processes. Particularly promising may be the development of methodology combining intramolecular carbon and hydrogen isotope abundances.

Stable isotope analysis on plant archives such as tree rings may convey information (*inter alia*) about plant acclimation and adaptation, and paleoclimate trends. This long-term perspective is inaccessible to manipulation and monitoring experiments yet crucial for the development of strategies to cope with climate change and overpopulation. The better we understand plant isotope fractionation, the more and the more precise information can be retrieved from archives. The present paper and recent studies on intramolecular $^{13}C/^{12}C$ signals (Wieloch *et al.*, 2018, 2021a,b) show that there is much room for improvement. Thus, we recommend pushing the development of intramolecular and dual-isotope methodology.

Current δD models describe metabolic fractionations as being constant (Roden *et al.*, 2000). As shown here, this is inadequate for plants grown under dry conditions where metabolic fractionations can exert predominant control over whole-molecule δD variability (Fig. 2d). Thus, to model plant D abundances over the whole range of environmental conditions,

metabolic fractionations need to be incorporated as variables which requires detailed knowledge about underlying processes.

Known metabolic fractionation processes cannot explain the signals reported here. Fractionation related to the photorespiration-to-photosynthesis ratio is located at glucose H^6 (Schleucher, 1998; Ehlers *et al.*, 2015). Moreover, *Picea abies* reportedly exhibits similar hydrogen exchange rates at tree-ring glucose H^1 and H^2 (≈40%) (Augusti *et al.*, 2006). Since *Pinus nigra* as a close relative can be expected to behave similarly, heterotrophic hydrogen exchange at these positions cannot cause pronounced deviations from slope=1 as observed for the δD_1-δD_2 regression (Fig. 2c). Therefore, we will now derive experimentally testable theories on the metabolic origins of the fractionation signals reported here.

Isotope fractionation related to sucrose-to-starch carbon partitioning

We report a large metabolic fractionation signals at tree-ring glucose H^2 (ε_{met} at H^2: *SD*≈±79‰, *range*≈260‰, *n*=31) which occurs upon the crossing of a response change point (Figs. 3a-c). At the leaf level, tree-ring glucose has two metabolic precursors, chloroplast starch and cytosolic sucrose. Growing *Phaseolus vulgaris* and *Spinacia oleracea* under optimal conditions, Schleucher *et al.* (1999) reported D depletions at glucose H^2 of leaf starch relative to sucrose of -333‰ and -500‰, respectively. This difference can be expected to contribute to the signal at tree-ring glucose H^2 via changes in sucrose-to-starch carbon partitioning as follows.

In plant leaves, net assimilated carbon is partitioned primarily into starch and sucrose (Fig. 4). Sucrose-to-starch carbon partitioning is controlled primarily by the rate of carbon assimilation (Sharkey *et al.*, 1985). Secondary control is exerted by C_i (Sharkey *et al.*, 1985), light (Sharkey *et al.*, 1985; Quick *et al.*, 1989), and water availability (Quick *et al.*, 1989, 1992; Vassey & Sharkey, 1989). Sucrose-to-starch carbon partitioning ratios were shown to increase with decreasing assimilation rates (Sharkey *et al.*, 1985), decreasing C_i (Sharkey *et al.*, 1985), decreasing light (Sharkey *et al.*, 1985; Quick *et al.*, 1989), and increasing drought (Quick *et al.*, 1989, 1992; Vassey & Sharkey, 1989). Reported responses are functionally coherent and qualitatively consistent across all species studied (*Phaseolus vulgaris* (Sharkey *et al.*, 1985; Vassey & Sharkey, 1989), *Spinacia oleracea* (Quick *et al.*, 1989), *Lupinus albus* (Quick *et al.*, 1992), *Helianthus annuus* (Quick *et al.*, 1992), *Vitis vinifera* (Quick *et al.*, 1992), *Eucalyptus globulus* (Quick *et al.*, 1992)). Furthermore, responses of sucrose-to-starch carbon partitioning

to ecophysiological changes reportedly exhibit change points. In leaves of *Phaseolus vulgaris*, the sucrose-to-starch carbon partitioning ratio was found to be largely constant at $C_i \geq 150$ ppm yet increases below this change point (from ≈0.5 to ≈4, SI 7) (Sharkey *et al.*, 1985). Thus, as C_i drops below the change point, the relative contribution of leaf sucrose to tree-ring glucose biosynthesis can be expected to increase. Thereby, tree-ring glucose H^2 will gradually approach the higher relative D abundance of leaf sucrose.

Isotope fractionation related to anaplerotic carbon flux into the Calvin-Benson cycle

Metabolic fractionation signals at tree-ring glucose H^1 and H^2 are closely related (Figs. 2a, and c). We propose this is due to (i) isotope fractionation related to anaplerotic carbon flux into the Calvin-Benson cycle (CBC) affecting both positions, and (ii) dependencies of both anaplerotic carbon flux into the CBC and sucrose-to-starch carbon partitioning on carbon assimilation.

Proposedly, the CBC is anaplerotically refilled by injection of five-carbon sugar phosphates from the oxidative branch of the stromal pentose phosphate pathway with glucose 6-phosphate (G6P) as precursor (Fig. 4) (Sharkey & Weise, 2016). According to these authors, primary flux control is exerted at the level of stromal PGI which catalyses interconversions between fructose 6-phosphate (F6P) and G6P. Under optimal growth conditions, the PGI reaction is strongly removed from equilibrium on the side of F6P resulting in low stromal G6P concentrations (Dietz, 1985; Gerhardt *et al.*, 1987; Kruckeberg *et al.*, 1989; Schleucher *et al.*, 1999). Allegedly, low G6P concentrations restrict the anaplerotic flux (Sharkey & Weise, 2016). As the carbon assimilation rate decreases below a change point (e.g., in response to low C_a, C_i, or light), the stromal PGI reaction shifts towards equilibrium and G6P concentrations increase (SI 8) (Dietz, 1985). With increasing G6P concentrations, anaplerotic flux into the CBC is believed to increase (Sharkey & Weise, 2016). This involves stromal glucose-6-phosphate dehydrogenase (G6PD, EC 1.1.1.49), the first enzyme of the pentose phosphate pathway. In the light, G6PD is downregulated via redox regulation by thioredoxin (Née *et al.*, 2009). However, downregulation can be allosterically reversed by increasing G6P concentrations (Cossar *et al.*, 1984; Preiser *et al.*, 2019). Thus, as carbon assimilation decreases below a change point, the PGI reaction shifts towards equilibrium and G6P concentrations increase which may cause increasing G6PD activity and anaplerotic flux.

Phaseolus vulgaris and *Spinacia oleracea* grown under optimal conditions exhibit pronounced D depletions at glucose H^2 of leaf starch relative to sucrose (see above) (Schleucher *et al.*,

1999). This depletion is caused by the stromal PGI reaction which was found to be more strongly removed from reaction equilibrium at [G6P]/[F6P]=3.31 than the cytosolic PGI reaction (Dyson & Noltmann, 1968; Schleucher *et al.*, 1999). Thus, as the stromal PGI reaction (with decreasing carbon assimilation) shifts towards equilibrium, H^2 of stromal G6P and its derivatives including leaf starch and tree-ring glucose can be expected to become less D depleted.

G6PD catalyses the irreversible conversion of G6P to 6-phosphogluconolactone. *In vitro*, the reaction was shown to have a strong D isotope effect of α=2.97 (Hermes *et al.*, 1982). Thus, upregulation of the anaplerotic flux (with decreasing carbon assimilation) can be expected to cause D enrichments at H^1 of stromal G6P and its derivatives.

Analysis of intramolecular $^{13}C/^{12}C$ ratios of the samples studied here has already provided evidence in support of anaplerotic flux into the CBC (Wieloch *et al.*, 2018). These authors explained a strong common ^{13}C signal at tree-ring glucose C-1 and C-2 by the anaplerotic flux. For shifts of the PGI reaction towards equilibrium, they predicted $^{13}C/^{12}C$ increases at C-1 and C-2 at a ratio of 2.25 and found a ratio of 2.74 (+1.35SE, -0.60SE) confirming their prediction. Interestingly, the reported ratio is somewhat higher than the predicted ratio yet not significantly. Still, the offset may be explained by the ^{13}C isotope effect of G6PD (α=1.0165) (Hermes *et al.*, 1982) which can be expected to cause an additional $^{13}C/^{12}C$ increase at C-1 of stromal G6P and its derivatives as anaplerotic flux increases.

Metabolic fractionation signals at H^1 and H^2: A general phenomenon in C_3 plants?

Cormier *et al.* (2018) grew six phylogenetically diverse angiosperms under varying C_a (grasses: *Arrhenatherum elatius* and *Festuca rubra*, legumes: *Trifolium pratense* and *Lathyrus pratensis*, forbs: *Centaurea jacea* and *Plantago lanceolata*; C_a=150, 280, 400, and 800 ppm). For leaf α-cellulose, these authors reported average whole-molecule ε_{met} increases of ≈20‰ in response to C_a decreases from 280 to 150 ppm yet no significant change above 280 ppm. Hence, their observations appear to be in line with ours (Tables 1-3, Figs. 3a-c).

However, our data show an average ε_{met} increase at tree-ring glucose H^1 and H^2 of up to 150‰ (Fig. 2b). Assuming ≈40% heterotrophic hydrogen exchanges as observed at these positions in *Picea abies* (Augusti *et al.*, 2006), we calculate an undiluted leaf-level increase of ≈250‰ (150‰/60*100) which corresponds to a whole-molecule increase of ≈70‰ (2*250‰/7). Thus,

ε_{met} increases in the gymnosperm *Pinus nigra* are considerably larger than the ≈20‰ angiosperm average effect reported by Cormier *et al.* (2018).

Unfortunately, whole-molecule data have a limited interpretability (*cf.* 'Introduction') and effects reported by Cormier *et al.* (2018) may be located at either of the seven H-C positions within α-cellulose glucose. For instance, a 20‰ whole-molecule effect may reflect a 140‰ effect at glucose H^6 due to a change of the photorespiration-to-photosynthesis ratio (*cf.* 'Introduction'). Thus, it remains uncertain whether the fractionation signals reported here occur generally in C_3 plants.

Table 1 Spearman's rank correlation coefficients and significance levels for relationships between ε_{met} and climate parameters within the period 1961 to 1995 (n=31).

	VPD	*PRE*	*PDSI*	*TMP*	*SD*	*RAD*	C_a	*SPEI 1*	*3*	*4*	*6*	*8*	*12*	*16*	*24*	*36*	*48*
Year	0.40	0.01	-0.51	0.45	0.12	0.28	0.58	-0.21	-0.25	-0.27	-0.30	-0.37	-0.46	-0.47	-0.58	-0.60	-0.57
Spring	0.54	-0.13	-0.55	0.55	0.09	0.18	---	-0.24	-0.19	-0.15	-0.16	-0.29	-0.34	-0.43	-0.58	-0.54	-0.55
Growing season	0.39	-0.04	-0.50	0.33	0.01	0.24	---	-0.26	-0.21	-0.20	-0.29	-0.31	-0.43	-0.47	-0.59	-0.61	-0.56
Summer	0.28	-0.04	-0.49	0.02	-0.17	0.10	---	-0.09	-0.20	-0.21	-0.25	-0.31	-0.43	-0.41	-0.56	-0.65	-0.55

ε_{met} denotes the average deuterium fractionation by metabolic processes at glucose H^1 and H^2 ($\pm SE$=3.5‰, $n \geq 3$). Raw data for the calculation of ε_{met} were acquired for tree-ring glucose of *Pinus nigra* laid down from 1961 to 1995 at a site in the Vienna basin. Climate parameters: air vapour pressure deficit, *VPD*; precipitation, *PRE*; the self-calibrating Palmer drought severity index, *PDSI* (Wells *et al.*, 2004); air temperature, *TMP*; sunshine duration, *SD*; global radiation, *RAD*; atmospheric CO_2 concentrations, C_a; the standardised precipitation-evapotranspiration index calculated for different timescales (1 to 48 months), *SPEI* (Vicente-Serrano *et al.*, 2010). Integration periods for the calculation of climate parameters: January to December, year; March to May, spring; March to November, growing season (Wieloch *et al.*, 2018); June to July, summer. Significance levels: <.05, light blue/light pink; <.01, blue/pink; <.001, dark blue/dark pink.

Table 2 Pearson correlation coefficients and significance levels for relationships between ε_{met} and climate parameters within the period 1983 to 1995 (n=13).

	VPD	*PRE*	*PDSI*	*TMP*	*SD*	*RAD*	C_a	*SPEI 1*	*3*	*4*	*6*	*8*	*12*	*16*	*24*	*36*	*48*
Year	0.26	-0.69	-0.51	-0.17	-0.12	-0.34	-0.73	-0.18	-0.20	-0.24	-0.28	-0.28	-0.10	0.03	0.03	-0.04	0.04
Spring	0.52	-0.71	-0.29	0.23	-0.08	-0.19	---	-0.28	-0.01	0.02	-0.08	-0.13	0.20	0.27	0.10	0.07	0.22
Growing season	0.27	-0.67	-0.52	-0.14	0.01	-0.33	---	-0.27	-0.17	-0.20	-0.29	-0.29	-0.18	0.03	0.02	-0.04	0.03
Summer	0.17	-0.67	-0.54	-0.47	-0.30	-0.51	---	-0.39	-0.44	-0.46	-0.31	-0.35	-0.29	-0.05	-0.03	-0.10	0.05

ε_{met} denotes the average deuterium fractionation by metabolic processes at glucose H^1 and H^2 ($\pm SE$=3.4‰, $n \geq 3$). Raw data for the calculation of ε_{met} were acquired for tree-ring glucose of *Pinus nigra* laid down from 1983 to 1995 at a site in the Vienna basin. Climate parameters: air vapour pressure deficit, *VPD*; precipitation, *PRE*; the self-calibrating Palmer drought severity index, *PDSI* (Wells *et al.*, 2004); air temperature, *TMP*; sunshine duration, *SD*; global radiation, *RAD*; atmospheric CO_2 concentrations, C_a; the standardised precipitation-evapotranspiration index calculated for different timescales (1 to 48 months), *SPEI* (Vicente-Serrano *et al.*, 2010). Integration periods for the calculation of climate parameters: January to December, year; March to May, spring; March to November, growing season (Wieloch *et al.*, 2018); June to July, summer. Significance levels: <.05, light blue; <.01, blue.

Table 3 Estimated coefficients of the ε_{met} change point model.

Coefficient	Estimate	SE*	Lower 95% CI	Upper 95% CI	p-value*
β_1	1801.97	479.02	863.10	2740.85	<.001
β_2	-0.56599	0.17577	-0.91051	-0.22147	<.01
β_3	-4.1851	1.4164	-6.9613	-1.4090	<.01
β_4	-1722.11	479.90	-2662.71	-781.51	<.001
β_5	0.58782	0.17749	0.23993	0.93571	<.001
β_6	4.2138	1.4574	1.3573	7.0703	<.01
e	-0.70310	0.05296	-0.80690	-0.59930	$<10^{-15}$

A change point model of the form $\varepsilon_{met}=\beta_1+\beta_2 z_1+\beta_3 z_2+\beta_4 I(x>e)+\beta_5 z_1 I(x>e)+\beta_6 z_2 I(x>e)$ was fitted to measured ε_{met} data (R^2=0.94, $p<10^{-15}$, n=31) (Fong *et al.*, 2017). ε_{met} denotes the average deuterium fractionation by metabolic processes at glucose H^1 and H^2 ($\pm SE$=3.5‰, $n\geq3$). Raw data for the calculation of ε_{met} were acquired for tree-ring glucose of *Pinus nigra* laid down from 1961 to 1995 at a site in the Vienna basin. β_1 to β_6, z_1, z_2, x, and e denote six model coefficients, March to June precipitation, annual atmospheric CO_2 concentration, the trend of the growing season 48-months *SPEI* used as change point variable (Fig. 3a, dotted black line), and the change point parameter, respectively. If x>e then I(x>e) equals 1, else I(x>e) equals 0. SE and CI denote the standard error and confidence interval, respectively. Asterisks mark estimations which assume that bootstrap sampling followed a normal distribution.

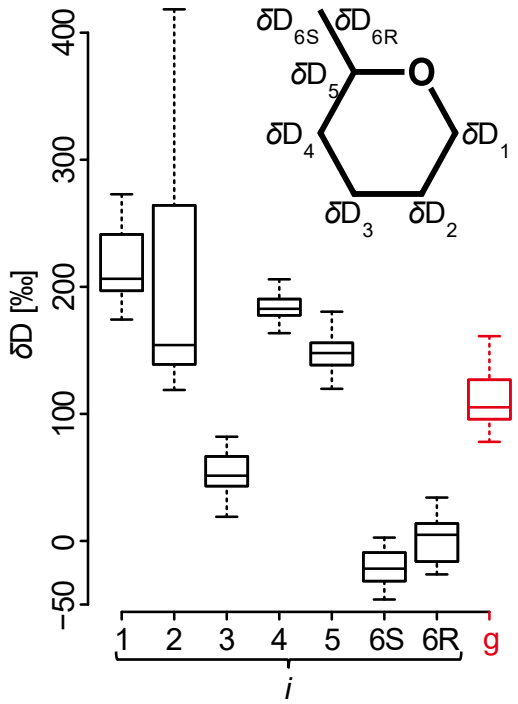

Figure 1 Variability in δD timeseries. δD_i and δD_g denote timeseries of D abundances at intramolecular H-C positions in tree-ring glucose (black) and of the whole molecule (red), respectively. Raw data were acquired for tree-ring glucose of *Pinus nigra* laid down from 1961 to 1995 at a site in the Vienna basin (δD_i: $\pm SE$=5.4‰, $n \geq 3$; δD_g: $\pm SE$=3.4‰, $n \geq 3$). Outliers were removed prior to analysis (δD_1 to δD_3: n=31, δD_4 and δD_5: n=30, δD_{6S}: n=26, δD_{6R}: n=28, δD_g: n=25). Data reference: Average D abundance of the methyl-group hydrogens of the glucose derivative used for NMR measurements. Insert: Glucose carbon skeleton showing intramolecular locations of δD_i timeseries.

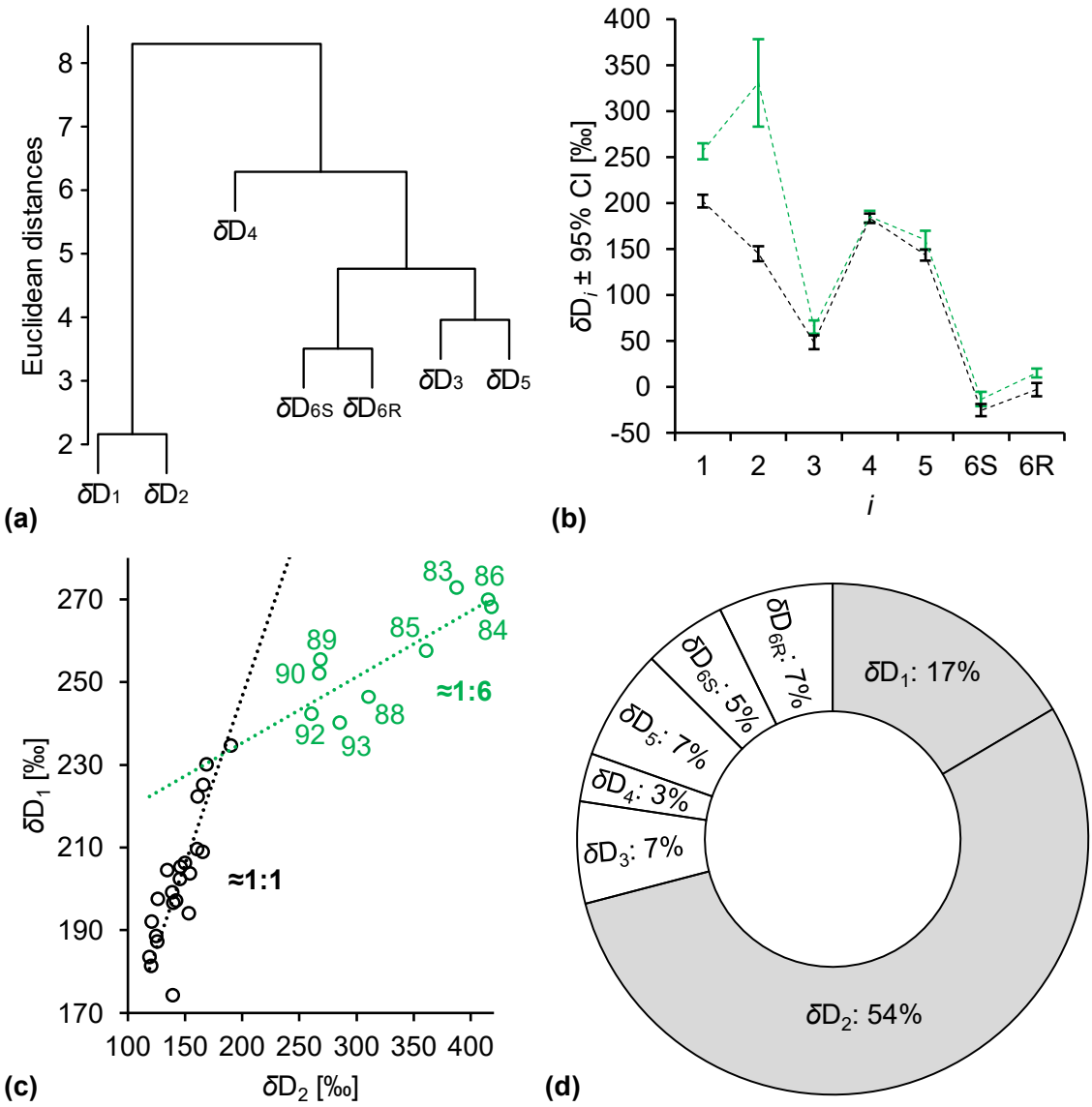

Figure 2 (a) Common variability among δD_i timeseries detected by Hierarchical Cluster Analysis (HCA). **(b)** Intramolecular δD_i patterns of the low- and high-value group (black and green, respectively). **(c)** Relationship between δD_1 and δD_2 (overall R^2=0.93, $p<10^{-15}$, n=31). Dotted lines: Linear major axis regression models showing that δD_1 and δD_2 increase at a 1:1 ratio at low values (black) and at a 1:6 ratio at high values (green). **(d)** Percent contributions of δD_i to the variance in δD_g. δD_i and δD_g denote timeseries of D abundances at intramolecular H-C positions in tree-ring glucose and of the whole molecule, respectively. Raw data were acquired for tree-ring glucose of *Pinus nigra* laid down from 1961 to 1995 at a site in the Vienna basin (δD_i: $\pm SE$=5.4‰, $n\geq3$; δD_g: $\pm SE$=3.4‰, $n\geq3$). Outliers were removed prior to analysis (δD_1 to δD_3: n=31, δD_4 and δD_5: n=30, δD_{6S}: n=26, δD_{6R}: n=28, δD_g: n=25). Low- and high-value group identified by HCA (SI 2). Figure 2b shows discrete data. Dashed lines added to

guide the eye. The variance partitioning analysis (2d) is based on years without missing data (n=8*25). Data reference: Average D abundance of the methyl-group hydrogens of the glucose derivative used for NMR measurements.

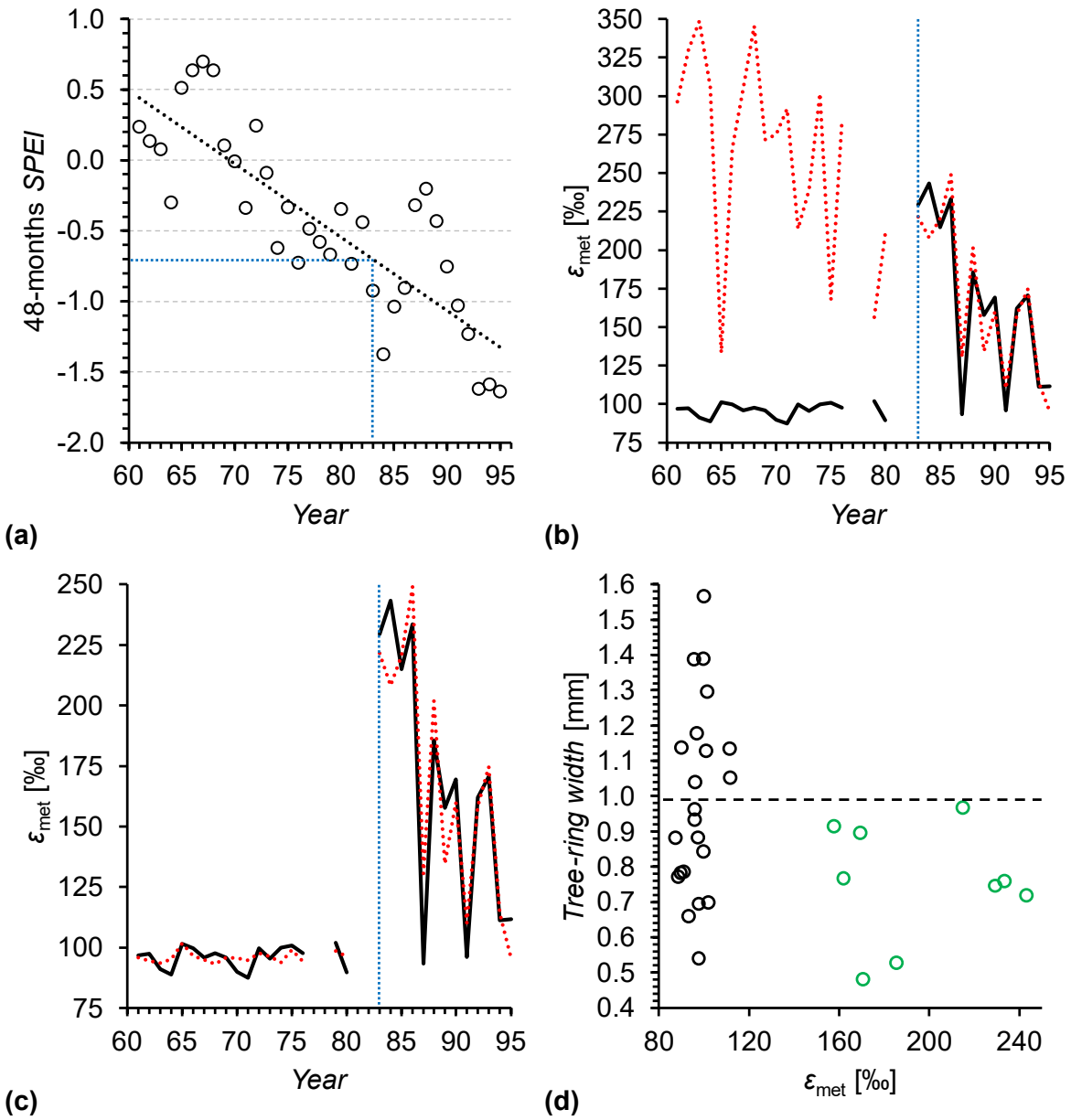

Figure 3 (a) Long-term development of growing season drought in the study region. Trendline analysis shows a significant increase in drought severity with shifts from "non-drought" from 1961 to 1978, to "mild drought" from 1979 to 1988, to "moderate drought" from 1989 to 1995 (dotted black line, R^2=0.69, $p<10^{-9}$, n=35). *SPEI* denotes the standardised precipitation-evapotranspiration index (Vicente-Serrano *et al.*, 2010). Here, it was calculated for the growing season (March to November (Wieloch *et al.*, 2018)) at 48.25° N, 16.25° E on a 48-months timescale indicative of long-term drought variability (black circles). Expressions of *SPEI* values indicate the drought severity as ≥-0.49, non-drought; -0.5 to -0.99, mild drought; -1 to -1.49, moderate drought; -1.5 to -1.99, severe drought; <-2, extreme drought (McKee *et al.*, 1993; Paulo *et al.*, 2012). **(b) and (c)** Comparison of measured (solid black line) and modelled (dotted red line) metabolic fractionation at glucose H^1 and H^2, ε_{met} (n=31). In (b), data were modelled

by a multivariate linear model without change point as ε_{met}=1802-0.566*PRE*-4.185C_a. In (c), data were modelled by a multivariate linear model with change point as ε_{met}=1802-0.566*PRE*-4.185C_a-1722*I(*trend*>-0.7031)+0.588*PRE**I(*trend*>-0.7031)+4.214C_a*I(*trend*>-0.7031). If *trend*>-0.7031 then I(*trend*>-0.7031) equals 1, else I(*trend*>-0.7031) equals 0. *PRE*, C_a, and *trend* denote March to July precipitation, annual atmospheric CO_2 concentration, and the long-term trend of the growing season 48-months *SPEI* (3a, dotted black line), respectively. Dotted blue line: Response change point as determined by the change point model. **(d)** Relationship between ε_{met} and *tree-ring width*. Green and black circles: Years in which the fractionating metabolic processes were upregulated and downregulated, respectively. Dashed line: Average tree-ring width of years in which the fractionating metabolic processes were downregulated (black circles, 0.99 mm). Tree-ring widths were measured for previous dendro-ecological studies (Leal *et al.*, 2008). Raw data for the calculation of ε_{met} were acquired for tree-ring glucose of *Pinus nigra* laid down from 1961 to 1995 at a site in the Vienna basin (±*SE*=3.5‰, $n \geq 3$).

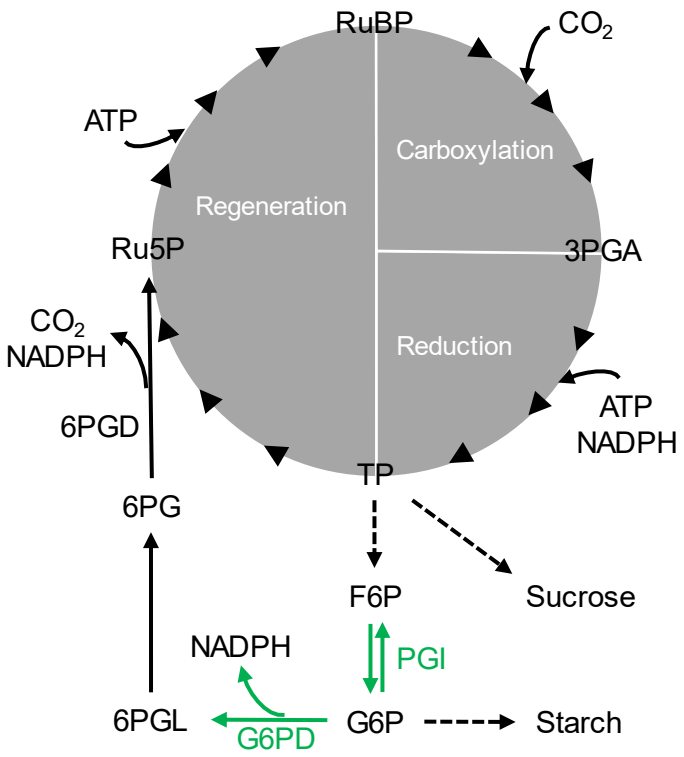

Figure 4 Sucrose-to-starch carbon partitioning and anaplerotic carbon flux into the Calvin-Benson cycle. Green: Enzyme reactions proposedly introducing D isotope signals at glucose H^1 and H^2. Enzymes: 6PGD, 6-phosphogluconate dehydrogenase; G6PD, glucose-6-phosphate dehydrogenase; PGI, phosphoglucose isomerase. Metabolites: 3PGA, 3-phosphoglycerate; 6PG, 6-phosphogluconate; 6PGL, 6-phosphogluconolactone; ATP, adenosine triphosphate; F6P, fructose 6-phosphate; G6P, glucose 6-phosphate; NADPH, nicotinamide adenine dinucleotide phosphate; Ru5P, ribulose 5-phosphate; RuBP, ribulose 1,5-bisphosphate; TP, triose phosphates (glyceraldehyde 3-phosphate, dihydroxyacetone phosphate).

Acknowledgements

For helpful discussions, we thank Thomas Cech (Austrian Research Centre for Forests), Youyi Fong (Fred Hutchinson Cancer Research Center, Seattle), Erhard Halmschlager (University of Natural Resources and Life Sciences, Vienna), John D. Marshall (SLU Umeå), John S. Roden (Southern Oregon University), Thomas D. Sharkey (Michigan State University), and Roland A. Werner (ETH Zürich). T.W.'s, I.E.'s, and J.S.'s research was funded by the Swedish Research Council VR (2013-05219, 2018-04456), the Knut and Alice Wallenberg Foundation ("NMR for Life" facility and grant 2015.0047) and the Kempe foundations.

Author contributions

T.W., and J.S. conceived the study. T.W. led the research. T.W., M.G., H.S., J.S., and I.E. collected and prepared the samples and acquired data. T.W., and J.Y. analysed the data. T.W. developed theories about the origin of reported isotope signals. T.W. wrote the paper with input from A.A., H.S., J.S., and J.Y.

Data availability

The data supporting the findings of this study are available from the corresponding author upon reasonable request.

References

Augusti A, Betson TR, Schleucher J. **2006**. Hydrogen exchange during cellulose synthesis distinguishes climatic and biochemical isotope fractionations in tree rings. *New Phytologist* **172**: 490–499.

Augusti A, Betson TR, Schleucher J. **2008**. Deriving correlated climate and physiological signals from deuterium isotopomers in tree rings. *Chemical Geology* **252**: 1–8.

Betson TR, Augusti A, Schleucher J. **2006**. Quantification of deuterium isotopomers of tree-ring cellulose using Nuclear Magnetic Resonance. *Analytical Chemistry* **78**: 8406–8411.

Cernusak LA, Barbour MM, Arndt SK, Cheesman AW, English NB, Feild TS, Helliker BR, Holloway-Phillips MM, Holtum JAM, Kahmen A, *et al.* 2016. Stable isotopes in leaf water of terrestrial plants. *Plant, Cell & Environment* **39**: 1087–1102.

Cormier M -A., Werner RA, Sauer PE, Gröcke DR, Leuenberger MC, Wieloch T, Schleucher J, Kahmen A. **2018**. ^{2}H-fractionations during the biosynthesis of carbohydrates

and lipids imprint a metabolic signal on the δ^2H values of plant organic compounds. *New Phytologist* **218**: 479–491.

Cossar JD, Rowell P, Stewart WDP. **1984**. Thioredoxin as a modulator of glucose-6-phosphate dehydrogenase in a N_2-fixing cyanobacterium. *Microbiology* **130**: 991–998.

Craig H, Gordon LI. **1965**. Deuterium and oxygen 18 variations in the ocean and the marine atmosphere. In: Tongiorgi E, ed. Pisa: Consiglio nazionale delle ricerche, Laboratorio di geologia nucleare, 9–130.

Dietz K-J. **1985**. A possible rate-limiting function of chloroplast hexosemonophosphate isomerase in starch synthesis of leaves. *Biochimica et Biophysica Acta* **839**: 240–248.

Dyson JE, Noltmann EA. **1968**. The effect of pH and temperature on the kinetic parameters of phosphoglucose isomerase. Participation of histidine and lysine in a proposed dual function mechanism. *The Journal of Biological Chemistry* **243**: 1401–1414.

Ehlers I, Augusti A, Betson TR, Nilsson MB, Marshall JD, Schleucher J. **2015**. Detecting long-term metabolic shifts using isotopomers: CO_2-driven suppression of photorespiration in C_3 plants over the 20th century. *Proceedings of the National Academy of Sciences of the United States of America* **112**: 15585–15590.

Evans JR, Farquhar GD, Sharkey TD, Berry JA. **1986**. Carbon isotope discrimination measured concurrently with gas exchange to investigate CO_2 diffusion in leaves of higher plants. *Australian Journal of Plant Physiology* **13**: 281–292.

Farquhar GD, Cernusak LA, Barnes B. **2007**. Heavy water fractionation during transpiration. *Plant Physiology* **143**: 11–18.

Farquhar GD, O'Leary MH, Berry JA. **1982**. On the relationship between carbon isotope discrimination and the intercellular carbon dioxide concentration in leaves. *Australian Journal of Plant Physiology* **9**: 121–137.

Flanagan LB, Comstock JP, Ehleringer JR. **1991**. Comparison of modeled and observed environmental influences on the stable oxygen and hydrogen isotope composition of leaf water in *Phaseolus vulgaris* L. *Plant Physiology* **96**: 588–596.

Fong Y, Huang Y, Gilbert PB, Permar SR. **2017**. chngpt: threshold regression model estimation and inference. *BMC Bioinformatics* **18**: 454.

Frank DC, Poulter B, Saurer M, Esper J, Huntingford C, Helle G, Treydte K, Zimmermann NE, Schleser GH, Ahlstrom A, *et al.* 2015. Water-use efficiency and transpiration across European forests during the Anthropocene. *Nature Climate Change* **5**: 579–583.

Gerhardt R, Stitt M, Heldt HW. **1987**. Subcellular metabolite levels in spinach leaves: Regulation of sucrose synthesis during diurnal alterations in photosynthetic partitioning. *Plant Physiology* **83**: 399–407.

Hermes JD, Roeske CA, O'Leary MH, Cleland WW. **1982**. Use of multiple isotope effects to determine enzyme mechanisms and intrinsic isotope effects. Malic enzyme and glucose 6-phosphate dehydrogenase. *Biochemistry* **21**: 5106–5114.

Kahmen A, Hoffmann B, Schefuß E, Arndt SK, Cernusak LA, West JB, Sachse D. **2013**. Leaf water deuterium enrichment shapes leaf wax n-alkane δD values of angiosperm plants II: Observational evidence and global implications. *Geochimica et Cosmochimica Acta* **111**: 50–63.

Köhler IH, Macdonald AJ, Schnyder H. **2016**. Last-century increases in intrinsic water-use efficiency of grassland communities have occurred over a wide range of vegetation composition, nutrient inputs, and soil pH. *Plant Physiology* **170**: 881.

Kruckeberg AL, Neuhaus HE, Feil R, Gottlieb LD, Stitt M. **1989**. Decreased-activity mutants of phosphoglucose isomerase in the cytosol and chloroplast of *Clarkia xantiana*. *The Biochemical Journal* **261**: 457–467.

Leal S, Eamus D, Grabner M, Wimmer R, Cherubini P. **2008**. Tree rings of *Pinus nigra* from the Vienna basin region (Austria) show evidence of change in climatic sensitivity in the late 20th century. *Canadian Journal of Forest Research* **38**: 744–759.

Leal S, Melvin TM, Grabner M, Wimmer R, Briffa KR. **2007**. Tree-ring growth variability in the Austrian Alps: the influence of site, altitude, tree species and climate. *Boreas* **36**: 426–440.

Loader NJ, Walsh RP, Robertson I, Bidin K, Ong RC, Reynolds G, McCarroll D, Gagen M, Young GH. **2011**. Recent trends in the intrinsic water-use efficiency of ringless rainforest trees in Borneo. *Philosophical Transactions of the Royal Society of London* **366**: 3330–3339.

Martin GJ, Zhang BL, Naulet N, Martin ML. **1986**. Deuterium transfer in the bioconversion of glucose to ethanol studied by specific labeling at the natural abundance level. *Journal of the American Chemical Society* **108**: 5116–5122.

McKee TB, Doesken NJ, Kleist J. **1993**. The relationship of drought frequency and duration to time scales. In: Proceedings of the 8th Conference on Applied Climatology. Anaheim, California: American Meteorological Society, 179–184.

Melander LCS, Saunders WH. **1980**. *Reaction rates of isotopic molecules*. New York: John Wiley & Sons.

Née G, Zaffagnini M, Trost P, Issakidis-Bourguet E. **2009**. Redox regulation of chloroplastic glucose-6-phosphate dehydrogenase: A new role for f-type thioredoxin. *FEBS Letters* **583**: 2827–2832.

Paulo AA, Rosa RD, Pereira LS. **2012**. Climate trends and behaviour of drought indices based on precipitation and evapotranspiration in Portugal. *Natural Hazards and Earth System Sciences* **12**: 1481–1491.

Peñuelas J, Canadell JG, Ogaya R. **2011**. Increased water-use efficiency during the 20th century did not translate into enhanced tree growth. *Global Ecology and Biogeography* **20**: 597–608.

Peñuelas J, Filella I. **2003**. Deuterium labelling of roots provides evidence of deep water access and hydraulic lift by *Pinus nigra* in a Mediterranean forest of NE Spain. *Environmental and Experimental Botany* **49**: 201–208.

Preiser AL, Fisher N, Banerjee A, Sharkey TD. **2019**. Plastidic glucose-6-phosphate dehydrogenases are regulated to maintain activity in the light. *Biochemical Journal* **476**: 1539–1551.

Quick WP, Chaves MM, Wendler R, David M, Rodrigues ML, Passaharinho JA, Pereira JS, Adcock MD, Leegood RC, Stitt M. **1992**. The effect of water stress on

photosynthetic carbon metabolism in four species grown under field conditions. *Plant, Cell & Environment* **15**: 25–35.

Quick P, Siegl G, Neuhaus E, Feil R, Stitt M. **1989**. Short-term water stress leads to a stimulation of sucrose synthesis by activating sucrose-phosphate synthase. *Planta* **177**: 535–546.

Roden JS, Ehleringer JR. **1999a**. Observations of hydrogen and oxygen isotopes in leaf water confirm the Craig-Gordon model under wide-ranging environmental conditions. *Plant Physiology* **120**: 1165–1174.

Roden JS, Ehleringer JR. **1999b**. Hydrogen and oxygen isotope ratios of tree-ring cellulose for riparian trees grown long-term under hydroponically controlled environments. *Oecologia* **121**: 467–477.

Roden JS, Ehleringer JR. **2000**. Hydrogen and oxygen isotope ratios of tree ring cellulose for field-grown riparian trees. *Oecologia* **123**: 481–489.

Roden JS, Lin G, Ehleringer JR. **2000**. A mechanistic model for interpretation of hydrogen and oxygen isotope ratios in tree-ring cellulose. *Geochimica et Cosmochimica Acta* **64**: 21–35.

Ross GJ. **2015**. Parametric and nonparametric sequential change detection in R: The cpm package. *Journal of Statistical Software* **1**.

Sade N, Gebremedhin A, Moshelion M. **2012**. Risk-taking plants: anisohydric behavior as a stress-resistance trait. *Plant Signaling & Behavior* **7**: 767–770.

Saurer M, Spahni R, Frank DC, Joos F, Leuenberger M, Loader NJ, McCarroll D, Gagen M, Poulter B, Siegwolf RTW, *et al.* 2014. Spatial variability and temporal trends in water-use efficiency of European forests. *Global Change Biology* **20**: 3700–3712.

Schleucher J. **1998**. Intramolecular deuterium distributions and plant growth conditions. In: Griffiths H, ed. Stable isotopes - Integration of biological, ecological and geochemical processes. Oxford: Bios Scientific Publishers, 63–73.

Schleucher J, Vanderveer P, Markley JL, Sharkey TD. **1999**. Intramolecular deuterium distributions reveal disequilibrium of chloroplast phosphoglucose isomerase. *Plant, Cell and Environment* **22**: 525–533.

Schmidt HL, Robins RJ, Werner RA. **2015**. Multi-factorial *in vivo* stable isotope fractionation: causes, correlations, consequences and applications. *Isotopes in Environmental and Health Studies* **51**: 155–199.

Schmidt H-L, Werner RA, Eisenreich W. **2003**. Systematics of ^{2}H patterns in natural compounds and its importance for the elucidation of biosynthetic pathways. *Phytochemistry Reviews* **2**: 61–85.

Sharkey TD, Berry JA, Raschke K. **1985**. Starch and sucrose synthesis in *Phaseolus vulgaris* as affected by light, CO_2, and abscisic acid. *Plant Physiology* **77**: 617–620.

Sharkey TD, Weise SE. **2016**. The glucose 6-phosphate shunt around the Calvin–Benson cycle. *Journal of Experimental Botany* **67**: 4067–4077.

Stokes A, Fourcaud T, Hruska J, Cermák J, Nadyezdhina N, Nadyezhdin V, Praus L. **2002**. An evaluation of different methods to investigate root system architecture of urban trees *in situ*: I. ground-penetrating radar. *Journal of Arboriculture* **28**: 2–10.

Strumia G, Wimmer R, Grabner M. **1997**. Dendroclimatic sensitivity of *Pinus nigra* Arnold in Austria. *Dendrochronologia* **15**: 129–137.

Vassey TL, Sharkey TD. **1989**. Mild water stress of *Phaseolus vulgaris* plants leads to reduced starch synthesis and extractable sucrose phosphate synthase activity. *Plant Physiology* **89**: 1066–1070.

Vicente-Serrano SM, Beguería S, López-Moreno JI. **2010**. A multiscalar drought index sensitive to global warming: The standardized precipitation evapotranspiration index. *Journal of Climate* **23**: 1696–1718.

Waterhouse JS, Switsur VR, Barker AC, Carter AHC, Robertson I. **2002**. Oxygen and hydrogen isotope ratios in tree rings: how well do models predict observed values? *Earth and Planetary Science Letters* **201**: 421–430.

Wells N, Goddard S, Hayes MJ. **2004**. A self-calibrating Palmer drought severity index. *Journal of Climate* **17**: 2335–2351.

Wieloch T, Ehlers I, Yu J, Frank D, Grabner M, Gessler A, Schleucher J. **2018**. Intramolecular ^{13}C analysis of tree rings provides multiple plant ecophysiology signals covering decades. *Scientific Reports* **8**: 5048.

Wieloch T, Sharkey TD, Werner RA, Schleucher J. **2021a**. Intramolecular $^{13}C/^{12}C$ signals inform about carbon allocation in plant leaves. https://doi.org/10.1101/2021.06.25.449710

Wieloch T, Werner RA, Schleucher J. **2021b**. Carbon flux around leaf-cytosolic glyceraldehyde-3-phosphate dehydrogenase introduces a ^{13}C signal in plant glucose. *Journal of Experimental Botany*. https://doi.org/10.1093/jxb/erab316

Wimmer R, Strumia G, Holawe F. **2000**. Use of false rings in Austrian pine to reconstruct early growing season precipitation. *Canadian Journal of Forest Research* **30**: 1691–1697.